Liu et al. Nanoscale Research Letters (2017) 12:586
DOI 10.1186/s11671-017-2350-z

Nanoscale Research Letters

NANO EXPRESS Open Access

The Coupling Effects of Surface Plasmon Polaritons and Magnetic Dipole Resonances in Metamaterials

Bo Liu[1†], Chaojun Tang[2*†], Jing Chen[3,4,5*†], Zhendong Yan[5], Mingwei Zhu[5], Yongxing Sui[1] and Huang Tang[1]

Abstract

We numerically investigate the coupling effects of surface plasmon polaritons (SPPs) and magnetic dipole (MD) resonances in metamaterials, which are composed of an Ag nanodisk array and a SiO_2 spacer on an Ag substrate. The periodicity of the Ag nanodisk array leads to the excitation of SPPs at the surface of the Ag substrate. The near-field plasmon interactions between individual Ag nanodisks and the Ag substrate form MD resonances. When the excitation wavelengths of SPPs are tuned to approach the position of MD resonances by changing the array period of Ag nanodisks, SPPs and MD resonances are coupled together into two hybridized modes, whose positions can be well predicted by a coupling model of two oscillators. In the strong coupling regime of SPPs and MD resonances, the hybridized modes exhibit an obvious anti-crossing, resulting into an interesting phenomenon of Rabi splitting. Moreover, the magnetic fields under the Ag nanodisks are greatly enhanced, which may find some potential applications, such as magnetic nonlinearity.

Keywords: Metamaterials, Plasmonics, Surface plasmon polaritons, Magnetic dipole resonances, Magnetic field enhancement

Background

It is well known that naturally occurring materials exhibit the saturation of the magnetic response beyond the THz regime. In light-matter interactions at optical frequencies, the magnetic component of light generally plays a negligible role, because the force exerted by the electric field on a charge is much larger than the force applied by the magnetic field, when light interacts with matter [1]. In the past few years, developing various metallic or dielectric nanostructures with appreciable magnetic response at optical frequencies has been a matter of intense study in the field of metamaterials. Recently, there is increasing interest in optical magnetic field characterization in nanoscale, although it remains a challenge because of the weak matter-optical magnetic field interactions [2]. At the same time, there have also been many efforts to obtain strong magnetic response with magnetic field enhancement in a wide spectrum range from visible [3–22] to infrared [23–44] regime. The physical mechanism underlining strong magnetic response is mainly the excitation of MD resonance in a variety of nanostructures including metal-insulator-metal (MIM) sandwich structures [3, 12, 16, 31, 32, 40], metallic split-ring resonators [29, 30, 36, 41, 42], high-refractive-index dielectric nanoparticles [14, 15, 17, 18, 20, 21], plasmonic nanoantennas [6, 8, 24–26, 28, 34, 37, 43], metamolecules [7, 9, 11, 13, 19, 33, 35, 38], and so on. To obtain strong magnetic response with magnetic field enhancement, MD resonance is also coupled to different narrow-band resonance modes with a high-quality factor, e.g., surface lattice resonances [4, 22, 39, 44], Fabry-Pérot cavity resonances [10, 23], Bloch surface waves [5], and Tamm plasmons [27]. A strong magnetic response with a great enhancement of magnetic fields at optical frequencies will have many potential applications, such as MD spontaneous emission [45–52], magnetic nonlinearity [53–56], optically controlled magnetic-field etching [57], magnetic optical Kerr effect [58], optical tweezers based on magnetic-field gradient [59, 60], circular dichroism (CD) measurement

* Correspondence: chaojuntang@126.com; jchen@njupt.edu.cn
Bo Liu, Chaojun Tang and Jing Chen contributed equally to this work.
†Equal contributors
[2]Center for Optics and Optoelectronics Research, Collaborative Innovation Center for Information Technology in Biological and Medical Physics, College of Science, Zhejiang University of Technology, Hangzhou 310023, China
[3]College of Electronic and Optical Engineering & College of Microelectronics, Nanjing University of Posts and Telecommunications, Nanjing 210023, China
Full list of author information is available at the end of the article

[61], etc. It is well known that plasmonic electric dipole resonance can hugely enhance electric fields in the vicinity of metal nanoparticles, and its coupling to SPPs can further enhance electric fields and generate other interesting physical phenomena. However, there are only a few researches on the coupling effects of SPPs and MD resonances.

In this work, we will numerically demonstrate the huge enhancement of magnetic fields at optical frequencies and the interesting phenomenon of Rabi splitting, due to the coupling effects of SPPs and MD resonances in metamaterials composed of an Ag nanodisk array and a SiO_2 spacer on an Ag substrate. The near-field plasmon interactions between individual Ag nanodisks and the Ag substrate form MD resonances. The periodicity of the Ag nanodisk array leads to the excitation of SPPs at the surface of the Ag substrate. When the excitation wavelengths of SPPs are tuned to approach the position of MD resonances by changing the array period of Ag nanodisks, SPPs and MD resonances are coupled together into two hybridized modes, whose positions can be well predicted by a coupling model of two oscillators. In the strong coupling regime of SPPs and MD resonances, the hybridized modes exhibit an obvious anticrossing, resulting into an interesting phenomenon of Rabi splitting. Moreover, the magnetic fields under the Ag nanodisks are greatly enhanced, which may find some potential applications, such as magnetic nonlinearity.

The unit cell of the designed metamaterials for the coupling effects of SPPs and MD resonances is schematically shown in Fig. 1. The Ag nanodisks lie on the *xy* plane, and the coordinate origin is supposed to be located at the center of the SiO_2 spacer. The incident light propagates in the negative *z*-axis direction, with its electric and magnetic fields along the *x*-axis and the *y*-axis directions, respectively. The reflection and absorption spectra and the electromagnetic field distributions are calculated by using the commercial software package "EastFDTD," which is based on finite difference time domain (FDTD) method [62]. In our numerical calculations, the refractive index of SiO_2 is 1.45, and the frequency-dependent relative permittivity of Ag is taken from experimental data [63]. This work mainly focuses on numerical investigation, but the designed metamaterials should be realized experimentally by the following procedures: the SiO_2 spacer is first coated on the Ag substrate through thermal evaporation, and then the Ag nanodisk array is fabricated on the SiO_2 spacer by some advanced nanofabrication technologies, such as electron beam lithography (EBL).

Methods

Figure 2 shows the calculated absorption and reflection spectra of a series of metamaterials under normal incidence of light, with the array period p_x along the *x*-axis direction

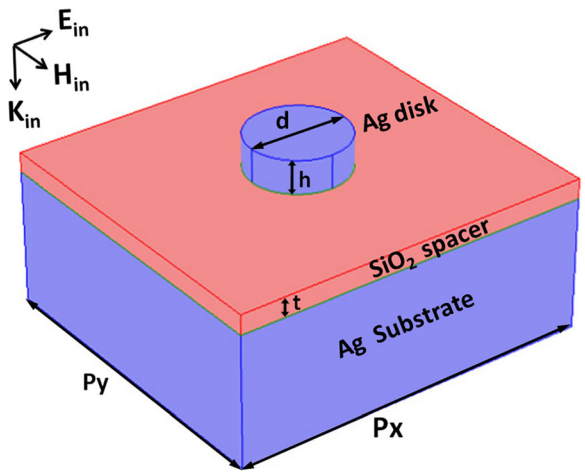

Fig. 1 Schematic of metamaterials composed of Ag nanodisks and a SiO_2 spacer on Ag substrate. Geometrical parameters: p_x and p_y are the array periods along the *x* and *y* directions, respectively; *t* is the thickness of the SiO_2 spacer; *d* and *h* are the diameter and the height of the Ag nanodisks. $\boldsymbol{E}_{in}$, $\boldsymbol{H}_{in}$, and $\boldsymbol{K}_{in}$ are the electric field, magnetic field, and wave vector of the incident light, which are along the *x*, *y*, and *z* axes, respectively

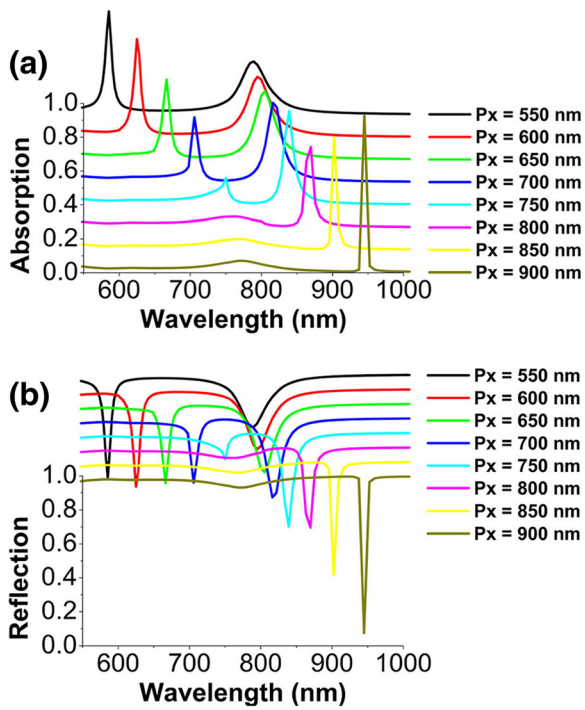

Fig. 2 Normal-incidence absorption (**a**) and reflection (**b**) spectra of metamaterials schematically shown in Fig. 1, in the wavelength range from 550 to 1000 nm. The array period p_x along the *x*-axis direction is varied from 550 to 900 nm in steps of 50 nm. The other geometrical parameters: d = 150 nm, h = 50 nm, t = 30 nm, and p_y = 500 nm. For clarity, individual spectra in **a** and **b** are vertically offset by 90 and 60% from one another, respectively

increased from 550 to 900 nm in steps of 50 nm. For each p_x, two resonance modes are found in the spectra, which result into the appearance of two absorption peaks and two reflection dips in Fig. 2a and b, respectively. The positions and bandwidths of two resonance modes are strongly dependent on the array period p_x. For p_x = 900 nm, the right sharp peak of absorption nearly reaches to 1. Such a strong light absorption in MIM structures is usually called as perfect absorption [64–66]. In addition, we have also investigated the effect of the array period p_y along the y-axis direction on the optical properties of metamaterials (not shown here). It is found that simultaneously changing p_y has no significant effect on the optical properties, except for the appearance of a high-order SPP mode when both p_x and p_y are increased to 700 nm. The high-order SPP mode will have an obvious red shift for the array period to be further increased. In Fig. 2, by keeping p_y = 500 nm unchanged, only the lowest order SPP mode propagating in the x-axis direction is excited in the spectral range of interest. In the following, we will demonstrate that these two resonance modes originate from the strong coupling between SPPs and MD resonances in the designed metamaterials.

In order to reveal the physical mechanism of two resonance modes in Fig. 2, we have proposed a coupling model of two oscillators to accurately predict the positions of two resonance modes for different array period p_x. In the coupling model, one of the oscillators is SPPs, and the other is MD. The strong coupling between SPPs and MD leads to the formation of two hybridized modes, i.e., the high- and low-energy states, whose energies can be calculated by the equation [67]:

$$E_{+,-} = (E_{\mathrm{MD}} + E_{\mathrm{SPPs}})/2 \pm \sqrt{\Delta/2 + (E_{\mathrm{MD}} - E_{\mathrm{SPPs}})^2/4}.$$

Here, E_{MD} and E_{SPPs} are the excitation energies of MD and SPPs, respectively; and Δ stands for the coupling strength. In Fig. 3, the open black circles show the positions of two resonance modes for different array period p_x, and the two branches of red lines give the corresponding results calculated by the coupled oscillator model with the coupling strength Δ = 100 meV. Obviously, the above model predicted well the positions of two resonance modes. This suggests that the appearance of two resonance modes in Fig. 2 is the result of the interaction of SPPs and MD in metamaterials.

The black diagonal line in Fig. 3 gives the excitation wavelengths of SPPs for different array period p_x, which is calculated by matching the reciprocal vector of the Ag nanodisk lattice with the momentum of SPPs under normal incidence [68]. The horizontal green line in Fig. 3 shows the position of MD mode, whose resonance wavelength is mainly determined by the size of Ag nanodisks and the thickness of the SiO_2 spacer, but is independent of the array periods. At the crossing of the two lines for

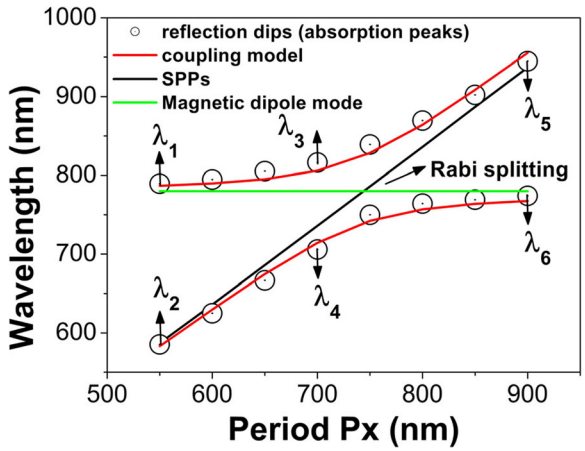

Fig. 3 Open black circles show the positions of absorption peaks or reflection dips in Fig. 2, and two red curved lines give the corresponding positions predicted by the coupling model of SPPs and MD mode. The resonance wavelengths of SPPs (black diagonal line) and MD mode (horizontal green line) are also presented

p_x = 750 nm, SPPs and MD are overlapped in positions, which are strongly coupled together. Therefore, the positions of two resonance modes in Fig. 2 exhibit an obvious anti-crossing, thus forming an interesting phenomenon of Rabi splitting [67]. Far away from the strong coupling regime, the positions of two resonance modes follow approximately one of the two lines.

Beside Rabi splitting, another effect of the strong coupling between SPPs and MD is the enhancement of magnetic fields. To exhibit this effect, in Fig. 4, we first plot the distributions of electromagnetic fields at the resonance wavelengths of λ_1 and λ_2 labeled in Fig. 3 for p_x = 550 nm. In this case, the positions of SPPs and MD are far, and their coupling is weak, as exhibited in Fig. 3. At the resonance wavelength of λ_1, the electric fields are highly confined near the edge of the Ag nanodisks and have two field "hotspots" on the left and right sides extending into the SiO_2 spacer (see Fig. 4a). The magnetic fields are concentrated within the SiO_2 spacer and have a maximum under the Ag nanodisks (see Fig. 4b). Such distribution properties of electromagnetic fields are mainly the typical characteristics of a MD resonance [69–71]. At the resonance wavelength of λ_2, parallel electromagnetic field bands stretching along the y-axis direction are formed, although they are disturbed near the Ag nanodisks (see Fig. 4c and d). In fact, such electromagnetic field distributions mainly correspond to the excitation of SPPs [68].

In Fig. 5, we plot the distributions of electromagnetic fields at the resonance wavelengths of λ_3 and λ_4 labeled in Fig. 3 for p_x = 700 nm. In this case, the positions of SPPs and MD are close, and their coupling becomes relatively stronger, as exhibited in Fig. 3. As a result, the

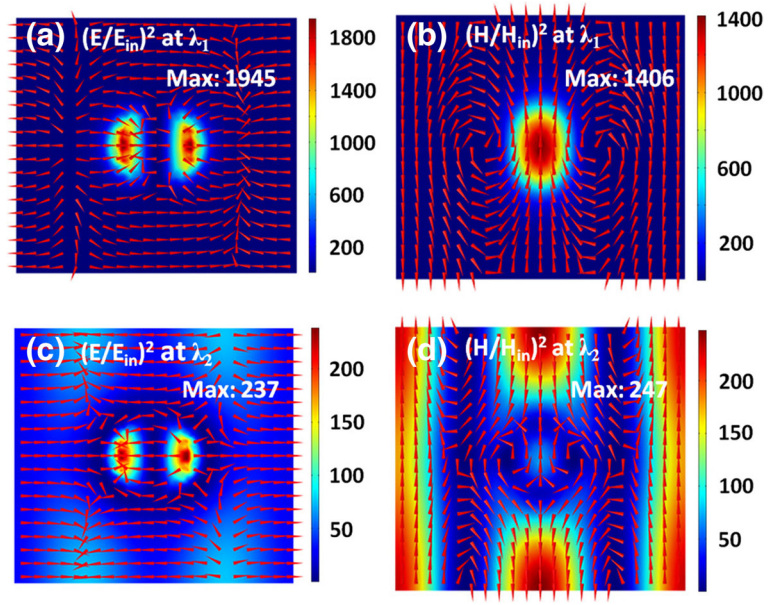

Fig. 4 a–d Normalized electric field intensity $(\boldsymbol{E}/\boldsymbol{E}_{in})^2$ and magnetic field intensity $(\boldsymbol{H}/\boldsymbol{H}_{in})^2$ on the *xoz* plane across the center of the SiO_2 spacers at the resonance wavelengths of λ_1 and λ_2 labeled in Fig. 3. Red arrows represent the field direction, and colors show the field strength

positions of two resonance modes are red-shifted from λ_1 and λ_2 to λ_3 and λ_4, respectively, and the electromagnetic fields near the Ag nanodisks are further enhanced. As clearly seen in Fig. 5a and b, at the resonance wavelength of λ_3, the maximum electric and magnetic fields are enhanced to be about 3500 and 2560 times of the incident field, which are 1.80 and 1.82 times stronger than the corresponding values at the resonance wavelengths of λ_1, respectively. In Fig. 5c and d, the maximum electric and magnetic fields at the resonance wavelength of λ_4 are enhanced to be about 1650 and 870 times of the incident field, which are 6.98 and 3.53 times stronger than the corresponding values at the resonance wavelengths of λ_2, respectively.

Figure 6 shows the electromagnetic field distributions at the resonance wavelengths of λ_5 and λ_6 labeled in Fig. 3 for p_x = 900 nm. The mixed mode at λ_5 has a very narrow bandwidth, as clearly seen in Fig. 2. As a result, its electromagnetic fields are hugely enhanced, with the maximum electric and magnetic fields exceeding 6500

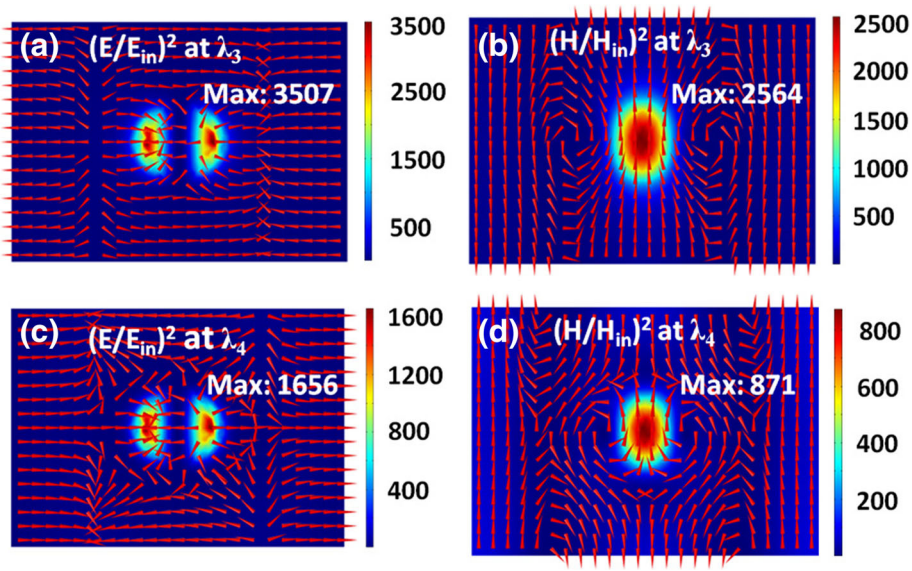

Fig. 5 a–d The same as in Fig. 4 but at the resonance wavelengths of λ_3 and λ_4 labeled in Fig. 3

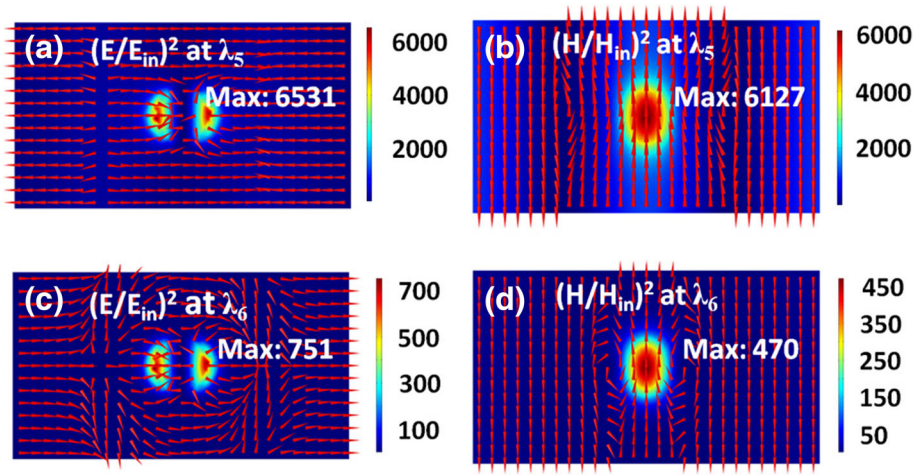

Fig. 6 a–d The same as in Fig. 4 but at the resonance wavelengths of λ_5 and λ_6 labeled in Fig. 3

and 6100 times of the incident fields, respectively. The huge enhancement of electromagnetic fields may find potential applications in nonlinear optics and sensing [72, 73]. In Fig. 6b, there exist three relatively weak field enhancement bands parallel in the *y*-axis direction and a pronounced field hotspot at the center. Such a field distribution directly indicates the hybridization feature of SPPs and MD. The mixed mode at λ_6 has a broad bandwidth, which has more component of MD than SPP, as indicated in Fig. 6c and d.

Conclusions

In this work, we have numerically investigated the coupling effects of SPPs and MD resonances in metamaterials, which are composed of an Ag nanodisk array and a SiO_2 spacer on an Ag substrate. The near-field plasmon interactions between individual Ag nanodisks and the Ag substrate form MD resonances. The periodicity of the Ag nanodisk array leads to the excitation of SPPs at the surface of the Ag substrate. When the excitation wavelengths of SPPs are tuned to be close to the position of MD resonances by varying the array period of Ag nanodisks, SPPs and MD resonances are coupled together into two hybridized modes, whose positions can be accurately predicted by a coupling model of two oscillators. In the strong coupling regime of SPPs and MD resonances, the hybridized modes exhibit an obvious anti-crossing and, thus, result into an interesting phenomenon of Rabi splitting. At the same time, the magnetic fields under the Ag nanodisks are enhanced greatly, which may find some potential applications, such as magnetic nonlinearity.

Acknowledgments

This work is financially supported by the National Natural Science Foundation of China (NSFC) under Grant Nos. 11304159, 11104136, and 11704184, the Natural Science Foundation of Zhejiang Province under Grant No. LY14A040004, the Natural Science Foundation of Jiangsu Province under Grant No. BK20161512, the Qing Lan Project of Jiangsu Province, the Open Project of State Key Laboratory of Millimeter Waves under Grant No. K201821, and the NUPTSF under Grant No. NY217045.

Authors' Contributions

BL, CT, and JC contributed equally to this work. BL, CT, and JC did the calculations. CT and JC wrote the manuscript. All authors read and approved the final manuscript.

Competing Interests

The authors declare that they have no competing interests.

Publisher's Note

Author details

[1]School of Mathematics and Physics, Jiangsu University of Technology, Changzhou 213001, China. [2]Center for Optics and Optoelectronics Research, Collaborative Innovation Center for Information Technology in Biological and Medical Physics, College of Science, Zhejiang University of Technology, Hangzhou 310023, China. [3]College of Electronic and Optical Engineering & College of Microelectronics, Nanjing University of Posts and Telecommunications, Nanjing 210023, China. [4]State Key Laboratory of Millimeter Waves, Southeast University, Nanjing 210096, China. [5]National Laboratory of Solid State Microstructures and Department of Materials Science and Engineering, Nanjing University, Nanjing 210093, China.

Received: 8 September 2017 Accepted: 24 October 2017
Published online: 09 November 2017

References

1. Burresi M, van Oosten D, Kampfrath T, Schoenmaker H, Heideman R, Leinse A, Kuipers L (2009) Probing the magnetic field of light at optical frequencies. Science 326:550–553
2. Rotenberg N, Kuipers L (2014) Mapping nanoscale light fields. Nat Photonics 8:919–926
3. Pakizeh T, Abrishamian MS, Granpayeh N, Dmitriev A, Käll M (2006) Magnetic-field enhancement in gold nanosandwiches. Opt Express 14:8240–8246
4. Tang CJ, Zhan P, Cao ZS, Pan J, Chen Z, Wang ZL (2011) Magnetic field enhancement at optical frequencies through diffraction coupling of magnetic plasmon resonances in metamaterials. Phys Rev B 83:041402(R)
5. Liu H, Sun XD, Pei YB, Yao FF, Jiang YY (2011) Enhanced magnetic response in a gold nanowire pair array through coupling with Bloch surface waves. Opt Lett 36:2414–2416
6. Zhou N, Kinzel EC, Xu XF (2011) Complementary bowtie aperture for localizing and enhancing optical magnetic field. Opt Lett 36:2764–2766

7. Wu PC, Chen WT, Yang KY, Hsiao CT, Sun G, Liu AQ, Zheludev NI, Tsai DP (2012) Magnetic plasmon induced transparency in three-dimensional metamolecules. Nano 1:131–138
8. Liu YM, Palomba S, Park Y, Zentgraf T, Yin XB, Zhang X (2012) Compact magnetic antennas for directional excitation of surface plasmons. Nano Lett 12:4853–4858
9. Lorente-Crespo M, Wang L, Ortuño R, García-Meca C, Ekinci Y, Martínez A (2013) Magnetic hot spots in closely spaced thick gold nanorings. Nano Lett 13:2654–2661
10. Xi Z, Lu YH, Yu WH, Yao PJ, Wang P, Ming H (2013) Strong coupling between plasmonic Fabry-Pérot cavity mode and magnetic plasmon. Opt Lett 38:1591–1593
11. Shafiei F, Monticone F, Le KQ, Liu XX, Hartsfield T, Alù A, Li XQ (2013) A subwavelength plasmonic metamolecule exhibiting magnetic-based optical Fano resonance. Nat Nanotechnol 8:95–99
12. Leong ESP, Liu YJ, Deng J, Fong YT, Zhang N, Wu SJ, Teng JH (2014) Fluid-enabled significant enhancement and active tuning of magnetic resonances in free-standing plasmonic metamaterials. Nano 6:11106–11111
13. Campione S, Guclu C, Ragan R, Capolino F (2014) Enhanced magnetic and electric fields via Fano resonances in metasurfaces of circular clusters of plasmonic nanoparticles. ACS Photonics 1:254–260
14. Zywietz U, Evlyukhin AB, Reinhardt C, Chichkov BN (2014) Laser printing of silicon nanoparticles with resonant optical electric and magnetic responses. Nat Commun 5:3402
15. Huang ZL, Wang JF, Liu ZH, Xu GZ, Fan YM, Zhong HJ, Cao B, Wang CH, Xu K (2015) Strong-field-enhanced spectroscopy in silicon nanoparticle electric and magnetic dipole resonance near a metal surface. J Phys Chem C 119:28127–28135
16. Verre R, Yang ZJ, Shegai T, Käll M (2015) Optical magnetism and plasmonic Fano resonances in metal-insulator-metal oligomers. Nano Lett 15:1952–1958
17. Bakker RM, Permyakov D, Yu YF, Markovich D, Paniagua-Domínguez R, Gonzaga L, Samusev A, Kivshar Y, Luk'yanchuk B, Kuznetsov AI (2015) Magnetic and electric hotspots with silicon nanodimers. Nano Lett 15:2137–2142
18. Mirzaei A, Miroshnichenko AE (2015) Electric and magnetic hotspots in dielectric nanowire dimmers. Nano 7:5963–5968
19. Bao YJ, Hu ZJ, Li ZW, Zhu X, Fang ZY (2015) Magnetic plasmonic Fano resonance at optical frequency. Small 11:2177–2181
20. Tribelsky MI, Miroshnichenko AE (2016) Giant in-particle field concentration and Fano resonances at light scattering by high-refractive-index particles. Phys Rev A 93:053837
21. Atakaramians S, Miroshnichenko AE, Shadrivov IV, Mirzaei A, Monro TM, Kivshar YS, Afshar VS (2016) Strong magnetic response of optical nanofibers. ACS Photonics 3:972–978
22. Chen J, Zha TQ, Zhang T, Tang CJ, Fan WF, Yu Y, Liu YJ, Zhang LB (2017) Enhanced magnetic fields at optical frequency by diffraction coupling of magnetic resonances in lifted metamaterials. J Lightwave Technol 35:71–74
23. Ameling R, Giessen H (2010) Cavity plasmonics: large normal mode splitting of electric and magnetic particle plasmons induced by a photonic microcavity. Nano Lett 10:4394–4398
24. Wang DX, Yang T, Crozier KB (2010) Charge and current reservoirs for electric and magnetic field enhancement. Opt Express 18:10388–10394
25. Grosjean T, Mivelle M, Baida FI, Burr GW, Fischer UC (2011) Diabolo nanoantenna for enhancing and confining the magnetic optical field. Nano Lett 11:1009–1013
26. Hou YM (2012) More electromagnetic energy converged by the assembly of magnetic resonator and antennas. Nano 4:874–878
27. Liu H, Sun XD, Yao FF, Pei YB, Huang F, Yuan HM, Jiang YY (2012) Optical magnetic field enhancement through coupling magnetic plasmons to Tamm plasmons. Opt Express 20:19160–19167
28. Gao Z, Shen LF, Li EP, Xu LL, Wang ZY (2012) Cross-diabolo nanoantenna for localizing and enhancing magnetic field with arbitrary polarization. J Lightwave Technol 30:829–833
29. Yu P, Chen SQ, Li JX, Cheng H, Li ZC, Tian JG (2013) Co-enhancing and -confining the electric and magnetic fields of the broken-nanoring and the composite nanoring by azimuthally polarized excitation. Opt Express 21:20611–20619
30. Yang Y, Dai HT, Sun XW (2013) Split ring aperture for optical magnetic field enhancement by radially polarized beam. Opt Express 21:6845–6850
31. Song ZY, Zhang BL (2014) Wide-angle polarization-insensitive transparency of a continuous opaque metal film for nearinfrared light. Opt Express 22:6519–6525
32. Sun S, Yi NB, Yao WJ, Song QH, Xiao SM (2014) Enhanced second-harmonic generation from nonlinear optical metamagnetics. Opt Express 22:26613–26620
33. Nazir A, Panaro S, Zaccaria RP, Liberale C, De Angelis F, Toma A (2014) Fano coil-type resonance for magnetic hot-spot generation. Nano Lett 14:3166–3171
34. Roxworthy BJ, Toussaint KC (2014) Simultaneously tuning the electric and magnetic plasmonic response using capped bi-metallic nanoantennas. Nano 6:2270–2274
35. Panaro S, Nazir A, Zaccaria RP, Razzari L, Liberale C, De Angelis F, Toma A (2015) Plasmonic moon: a Fano-like approach for squeezing the magnetic field in the infrared. Nano Lett 15:6128–6134
36. Alizadeh MH, Reinhard BM (2015) Plasmonically enhanced chiral optical fields and forces in achiral split ring resonators. ACS Photonics 2:361–368
37. Hasan D, Ho CP, Pitchappa P, Lee C (2015) Dipolar resonance enhancement and magnetic resonance in cross-coupled bow-tie nanoantenna array by plasmonic cavity. ACS Photonics 2:890–898
38. Hu DJ, Wang P, Pang L, Gao FH, Du JL (2015) Pure magnetic resonances controlled by the relative azimuth angle between meta-atoms. Opt Express 23:17675–17686
39. Chen J, Mao P, Xu RQ, Tang CJ, Liu YJ, Wang QG, Zhang LB (2015) Strategy for realizing magnetic field enhancement based on diffraction coupling of magnetic plasmon resonances in embedded metamaterials. Opt Express 23: 16238–16245
40. Xiang YX, Luo WW, Cai W, Ying CF, Yu XY, Zhang XZ, Liu H, Xu JJ (2016) Ultra-strong enhancement of electromagnetic fields in an L-shaped plasmonic nanocavity. Opt Express 24:3849–3857
41. Zhou F, Wang C, Dong BQ, Chen XF, Zhang Z, Sun C (2016) Scalable nanofabrication of U-shaped nanowire resonators with tunable optical magnetism. Opt Express 24:6367–6380
42. Yong ZD, Zhang SL, Gong CS, He SL (2016) Narrow band perfect absorber for maximum localized magnetic and electric field enhancement and sensing applications. Sci Rep 6:24063
43. Chen Y, Chen YH, Chu JR, Xu XF (2017) Bridged bowtie aperture antenna for producing an electromagnetic hot spot. ACS Photonics 4:567–575
44. Chen J, Fan WF, Zhang T, Tang CJ, Chen XY, Wu JJ, Li DY, Ying Y (2017) Engineering the magnetic plasmon resonances of metamaterials for high-quality sensing. Opt Express 25:3675–3681
45. Feng TH, Zhou Y, Liu DH, Li JS (2011) Controlling magnetic dipole transition with magnetic plasmonic structures. Opt Lett 36:2369–2371
46. Taminiau TH, Karaveli S, van Hulst NF, Zia R (2012) Quantifying the magnetic nature of light emission. Nat Commun 3:979
47. Decker M, Staude I, Shishkin II, Samusev KB, Parkinson P, Sreenivasan VKA, Minovich A, Miroshnichenko AE, Zvyagin A, Jagadish C, Neshev DN, Kivshar YS (2013) Dual-channel spontaneous emission of quantum dots in magnetic metamaterials. Nat Commun 4:2949
48. Hein SM, Giessen H (2013) Tailoring magnetic dipole emission with plasmonic split-ring resonators. Phys Rev Lett 111:026803
49. Mivelle M, Grosjean T, Burr GW, Fischer UC, Garcia-Parajo MF (2015) Strong modification of magnetic dipole emission through diabolo nanoantennas. ACS Photonics 2:1071–1076
50. Cui L, Huang MY, You YM, Li GM, Zhang YJ, Liu CK, Liu SL (2016) Enhancement of magnetic dipole emission at yellow light with polarization-independent hexagonally arrayed nanorods optical metamaterials. Opt Mater Express 6:1151–1160
51. Feng TH, Xu Y, Liang ZX, Zhang W (2016) All-dielectric hollow nanodisk for tailoring magnetic dipole emission. Opt Lett 41:5011–5014
52. Baranov DG, Savelev RS, Li SV, Krasnok AE, Alù A (2017) Modifying magnetic dipole spontaneous emission with nanophotonic structures. Laser Photon Rev 11:1600268
53. Klein MW, Enkrich C, Wegener M, Linden S (2006) Second-harmonic generation from magnetic metamaterials. Science 313:502–504
54. Kolmychek IA, Bykov AY, Mamonov EA, Murzina TV (2015) Second-harmonic generation interferometry in magnetic-dipole nanostructures. Opt Lett 40: 3758–3761
55. Litchinitser NM, Sun JB (2015) Optical meta-atoms: going nonlinear. Science 350:1033–1034
56. Kuznetsov AI, Miroshnichenko AE, Brongersma ML, Kivshar YS, Luk'yanchuk B (2016) Optically resonant dielectric nanostructures. Science 354:aag2472
57. Yatsui T, Tsuboi T, Yamaguchi M, Nobusada K, Tojo S, Stehlin F, Soppera O, Bloch D (2016) Optically controlled magnetic-field etching on the nano-scale. Light Sci Appl 5:e16054

58. Armelles G, Caballero B, Cebollada A, Garcia-Martin A, Meneses-Rodríguez D (2015) Magnetic field modification of optical magnetic dipoles. Nano Lett 15:2045–2049
59. Shi L, Meseguer F (2012) Magnetic interaction in all silicon waveguide spherical coupler device. Opt Express 20:22616–22626
60. Liberal I, Ederra I, Gonzalo R, Ziolkowski RW (2014) Magnetic dipole super-resonances and their impact on mechanical forces at optical frequencies. Opt Express 22:8640–8653
61. Yoo S, Cho M, Park QH (2014) Globally enhanced chiral field generation by negative-index metamaterials. Phys Rev B 89:161405(R)
62. Website: www.eastfdtd.com
63. Johnson PB, Christy RW (1972) Optical constants of the noble metals. Phys Rev B 6:4370–4379
64. Liu ZQ, Liu XS, Huang S, Pan PP, Chen J, Liu GQ, Gu G (2015) Automatically acquired broadband plasmonic-metamaterial black absorber during the metallic film-formation. ACS Appl Mater Interfaces 7:4962–4968
65. Liu ZQ, Liu GQ, Fu GL, Liu XS, Wang Y (2016) Multi-band light perfect absorption by a metal layer-coupled dielectric metamaterial. Opt Express 24:5020–5025
66. Liu GQ, Nie YY, Fu GL, Liu XS, Liu Y, Tang L, Liu ZQ (2017) Semiconductor meta-surface based perfect light absorber. Nanotechnology 28:165202
67. Bonnand C, Plenet JC, Bréhier A, Parashkov R, Lauret JS, Deleporte E, Bellessa J (2008) Particularities of surface plasmon-exciton strong coupling with large Rabi splitting. New J Phys 10:065017
68. Dan'ko V, Dmitruk M, Indutnyi I, Mamykin S, Myn'ko V, Shepeliavyi P, Lukaniuk M, Lytvyn P (2017) Au gratings fabricated by interference lithography for experimental study of localized and propagating surface plasmons. Nanoscale Res Lett 12:190
69. Hao J, Wang J, Liu X, Padilla WJ, Zhou L, Qiu M (2010) High performance optical absorber based on a plasmonic metamaterial. Appl Phys Lett 96:251104
70. Tang CJ, Yan ZD, Wang QG, Chen J, Zhu MW, Liu B, Liu FX, Sui CH (2015) Ultrathin amorphous silicon thin-film solar cells by magnetic plasmonic metamaterial absorbers. RSC Adv 5:81866–81874
71. Wu D, Liu YM, Li RF, Chen L, Ma R, Liu C, Ye H (2016) Infrared perfect ultra-narrow band absorber as plasmonic sensor. Nanoscale Res Lett 11:483
72. Liu ZQ, Fu GL, Huang ZP, Chen J, Liu XS (2017) Multi-band ultra-sharp transmission response in all-dielectric resonant structures containing Kerr nonlinear media. Plasmonics 12:577–582
73. Liu ZQ, Fu GL, Liu XS, Liu Y, Tang L, Liu ZM, Liu GQ (2017) High-quality multispectral bio-sensing with asymmetric all-dielectric meta-materials. J Phys D Appl Phys 50:165106